Proc. Sixth Int. Symp. Polar. Phenom. in Nucl. Phys., Osaka, 1985
J. Phys. Soc. Jpn. 55 (1986) Suppl. p. 322-326

# Folding Model for Intermediate-Energy Deuteron Scattering

M. Yahiro, H. Kameyama*, Y. Iseri*, M. Kamimura* and M. Kawai*

Shimonoseki University of Fisheries, Shimonoseki 759-65, Japan
*Department of Physics, Kyushu University, Fukuoka 812, Japan

Abstract

The deuteron elastic scattering from $^{58}$Ni at 400 MeV is analyzed with the single-folding potential which is constructed from the nucleon optical potentials at 200 MeV. Two typies of nucleon optical potentials are examined: (a) a standard, Woods-Saxon type and (b) a non Woods-Saxon type of Schroedinger-equation form of Dirac phenomenology. The folding potential with (b) gives definitely better agreement with the experimental data at forward angles up to 15° than the one with (a). The key to the success of the folding model with (b) seems to be the wine-bottle shaped real central part which is much more weakly attractive than the latter.

Accurate quantum description of the deuteron (d) elastic scattering is an important theme of the nuclear reaction theory as the scattering of the simplest composite projectile. The scattering at lower incident energies, say $T_d \lesssim 100$ MeV, have been analyzed first with a single-folding model [1] in which the deuteron potential is calculated by a folding of the optical potentials for proton (p) and neutron (n) into the deuteron ground state density. This model, however, has been unable to reproduce the experimental data in this energy range.[1,2] The problem has been solved by the introduction of the deuteron breakup process into the model.[3]

As the incident energy $T_d$ increases, however, the deuteron breakup effect becomes less important, and the folding model is expected to be valid on the whole. We have applied the model to an analysis of recent data from Saclay[4] on the deuteron elastic scattering from $^{40}$Ca and $^{58}$Ni at intermediate energies, $T_d$=200∿700 MeV. We report here the result on d+$^{58}$Ni scattering at $T_d$=400 MeV.

The single folding potential, $U_d$, is defined by

$$U_d = \langle \chi_d \mid U_p + U_n + V_c \mid \chi_d \rangle \tag{1}$$

where $U_n$ stands for the neutron optical potential, $U_p$ and $V_c$ for the nuclear and Coulomb parts of the proton optical potential respectively, and $\chi_d$ for the deuteron internal wave function calculated with the Reid soft-core p-n interaction potential.[5] We neglect the coupling due to $V_c$ between the S- and D-state parts of $\chi_d$. The Schroedinger equation including $U_d$ is solved with the relativistic kinematics.[6]

At $T_d$=400 MeV, $U_d$ is constructed from $U_p$ and $U_n$ for the incident energy of $T_{p,n}$= 200 MeV, since each nucleon in the deuteron has the highest probability of having half the deuteron kinetic energy. As experimental data are not available on the p+$^{58}$Ni elastic scattering at 200 MeV, we take the following procedure to determine the corresponding optical potentials.

First we search a proton optical potential to fit the data on the p+$^{40}$Ca scattering at 200 MeV. We then extrapolate it with the mass number and the proton number of the target nucleus to the p+$^{58}$Ni case, keeping the depth and geometrical parameters constant. This procedure is expected to be reliable, since it works very well at $T_p \simeq$ 180 MeV, i.e. between the p+$^{40}$Ca scattering at 181 MeV[7] and the p+$^{58}$Ni scattering at 178 MeV[8] for both of which experimental data are available. The neutron optical potential is assumed to be the same as the proton one except the charge of the projectile.

The procedure is used first to determine a standard Woods-Saxon (WS) type proton optical potential, $U_p$(WS) for p+$^{58}$Ni at 200 MeV. In the search of the proton optical potential for the p+$^{40}$Ca scattering at 200 MeV, the starting parameters are taken from Ref.7. Relativistic effects are treated approximately as in Ref.6. The resulting parameters are shown in Table.I. The same parameters are used for $U_p$(WS), and $U_n$(WS) for p+$^{58}$Ni as mentioned. They are folded to give a deuteron optical potential $U_d$(WS).

Figure 1 shows the cross section, $\sigma$, and the vector- and tensor-analyzing powers,

Table I. Parameters of the best fit Woods-Saxon type potential for $^{40}Ca(p,p)^{40}Ca$ and $^{58}Ni(p,p)^{58}Ni$ at 200 MeV. All lengths are given in fm and potentials in MeV.

| $V_0$ | $r_R$ | $a_R$ | $W_V$ | $r_I$ | $a_I$ | $V_{so}$ | $r_R^{so}$ | $a_R^{so}$ | $W_{so}$ | $r_I^{so}$ | $a_I^{so}$ |
|---|---|---|---|---|---|---|---|---|---|---|---|
| 14.21 | 1.305 | 0.7101 | 13.90 | 1.142 | 0.7305 | 2.596 | 0.9960 | 0.6650 | -1.856 | 1.019 | 0.5529 |

$$U_p(WS)=-[V_0 f(r_R,a_R)+iW_V f(r_I,a_I)]+\frac{2d}{rdr}[V_{so} f(r_R^{so},a_R^{so})+iW_{so} f(r_I^{so},a_I^{so})]\sigma\cdot L$$

$$f(r_0,a)=1/(1+\exp((r-r_0A^{1/3})/a))$$

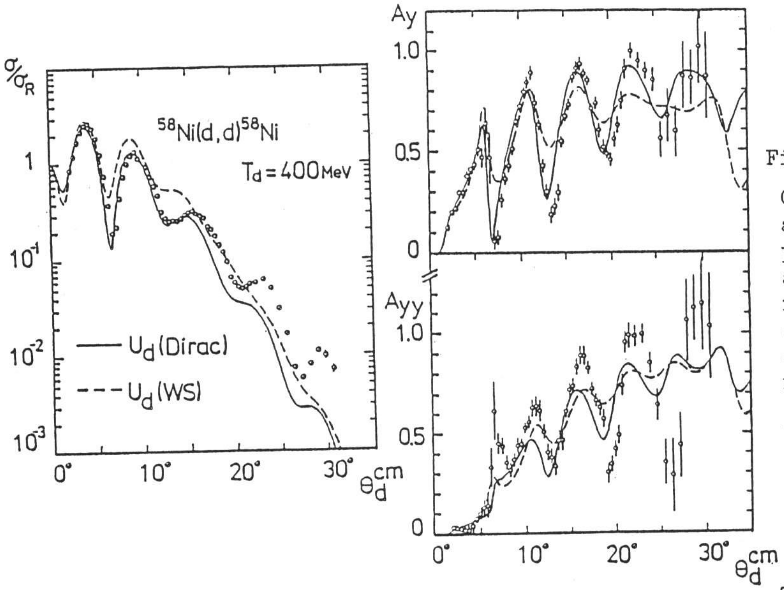


Figure 1.

Cross section and vector- and tensor-analyzing powers in $^{58}Ni(d,d)^{58}Ni$ at $T_d$=400 MeV. The dots represent the experimental data[4] and the lines are obtained with the folding model calculations. The solid line corresponds to $U_d$(Dirac) and the dashed line to $U_d$(WS).

$A_y$ and $A_{yy}$ respectively, for the deuteron scattering from $^{58}Ni$ at 400 MeV. The dashed lines represent the result of the folding potential, $U_d$(WS). The experimental data[4] are represented by dots. One sees that the dashed lines fail to reproduce the data, expecially the strong oscillation of $A_y$ and $A_{yy}$.

To solve the problem, we note that the data on the p+$^{40}Ca$ scattering at 200 MeV does not uniquely determine the optical potential. In fact, one can find a Dirac optical model potential[9,10] which gives an equaly good fit to the data as the WS type potential. The model gives a non-WS type potential

$$U_p(\mathrm{Dirac})=U_0+\frac{m}{E_p}U_s-\frac{1}{2E_p}(U_0^2-U_s^2)-\frac{1}{2E_p}V_c(V_c+2U_0)+U_{\mathrm{Darwin}}-\frac{1}{2E_pBr}\frac{dB}{dr}(\sigma\cdot L) \tag{2}$$

in its Schroedinger-equation form

$$\left[-\frac{\nabla^2}{2E_p}+U_p(\mathrm{Dirac})+V_c-\frac{E_p^2-m^2}{2E_p}\right]\phi=0 \tag{3}$$

for the function $\phi$ which is related to the upper two components, $\Psi_u$, of the Dirac wave function through $\Psi_u=\sqrt{B}\phi$. In Eqs.(2) and (3), all the notations are the same as in Ref. 9 : $E_p$ is the proton total energy in the c.m. system, $U_s$ the Lorentz-scalar potential, $U_0$ the time-like component of the Lorentz-vector potential, $B=(E+m+U_s-U_0-V_c)/(E+m)$ and $U_{Darwin}$ is the so-called Darwin term. The first and the fourth term in Eq.(3) give effectively almost the same relativistic kinematical corrections as the one used in the standard WS analysis.[6] The depth and geometrical parameters of $U_s$ and $U_0$ are searched to fit the experimental data. The starting parameters are taken from Ref. 9. The resulting parameters are in Table II, and the calculated results are shown by the solid lines in Fig.2. The same parameters are used for the potential $U_p$(Dirac) for the p+$^{58}Ni$ scattering at 200 MeV, as mentioned above, and for the corresponding neutron potential $U_n$(Dirac). It should be noted that $U_n$(Dirac) is slightly different from $U_p$(Dirac) by a "Coulomb correction" term, $(1/2E_p)V_c(V_c+2U_0)$.

For the p+$^{40}Ca$ scattering at 200 MeV, the Dirac optical model potential is much more weakly attractive than the Woods-Saxon type potential. The large difference between the two potentials represents the ambiguity of the optical potential for the proton scattering.

Table II. Parameters of $U_0$ and $U_S$ in the best fit Dirac optical model for $^{40}Ca(p,p)^{40}Ca$ and $^{58}Ni(p,p)^{58}Ni$ at 200 MeV. All lengths are given in fm and potentials in MeV.

| $V_0$ | $r_{0R}$ | $a_{0R}$ | $W_0$ | $r_{0I}$ | $a_{0I}$ | $V_S$ | $r_{SR}$ | $a_{SR}$ | $W_S$ | $r_{SI}$ | $a_{SI}$ |
|---|---|---|---|---|---|---|---|---|---|---|---|
| 344.6 | 1.016 | 0.6680 | -82.56 | 1.053 | 0.6010 | -466.3 | 1.004 | 0.6949 | 65.60 | 1.075 | 0.5201 |

$U_p$(Dirac) : $U_0=V_0 f(r_{0R},a_{0R})+iW_0 f(r_{0I},a_{0I})$ , $U_S=V_S f(r_{SR},a_{SR})+iW_S f(r_{SI},a_{SI})$

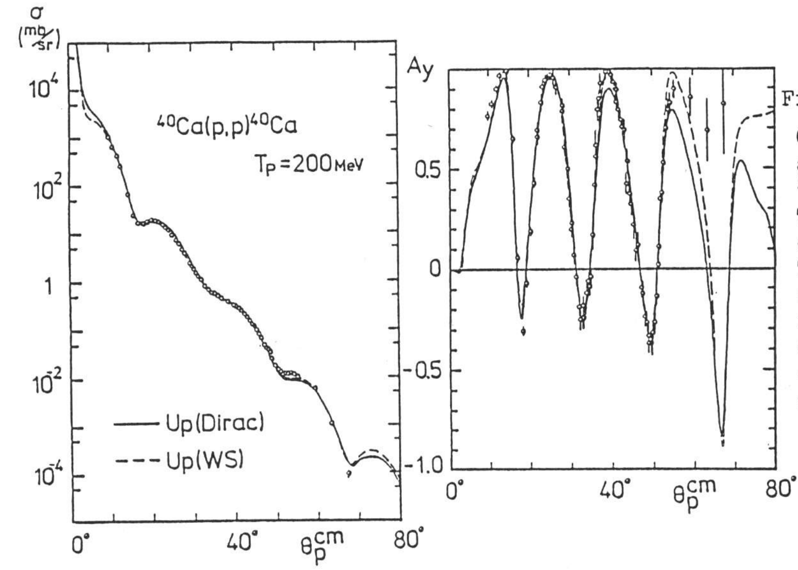


Figure 2.
Cross section and vector analyzing power for $^{40}Ca(p,p)^{40}Ca$ at 200 MeV. The dots represent the experimental data <10>. The solid and dashed lines are results of the best fit Dirac optical model and Woods-Saxon type optical potentials respectively.

In Fig.1, the solid line shows the result of $U_d$(Dirac) which is constructed from $U_p$(Dirac) and $U_n$(Dirac). It is obvious that $U_d$(Dirac) is superior to $U_d$(WS) in the agreement with the data. Especially, $U_d$(Dirac) well reproduces the data on $A_y$. Even for σ, $U_d$(Dirac) gives very good agreement at forward angles up to 15°, while $U_d$(WS) failes to do so. At angles larger than 15°, however, the agreement of $U_d$(Dirac) with the data is not sufficient especially for the cross sections;$U_d$(Dirac) does not reproduce the magnitude, although it reproduces the position of the maxima and the mimima.

The radial dependence of $U_d$(Dirac) is compared with that of $U_d$(WS) in Fig.3. We note a large difference between the two potentials especially in the real central part; $U_d$(Dirac) has a wine-bottle shaped one with a much weaker attraction than that of $U_d$(WS). The effect of this difference can be seen if one performs a calculation with $U_d$(WS) with its real central part replaced by that of $U_d$(Dirac). The result is shown in Fig.4 by a solid line. It shows a much stronger oscillation in $A_y$ and $A_{yy}$ than the result of $U_d$(WS) shown in Fig.1. Such a large change in $A_y$ and $A_{yy}$ does not arise even if one replaces either the imaginary central part or the spin-orbit part of $U_d$(WS) by the corresponding components of $U_d$(Dirac), as one sees from the dashed and dotted lines in Fig.4. Thus one sees that the real central part of $U_d$(Dirac) is essential for the reproduction of the experimentally observed strong oscillation in $A_y$ and $A_{yy}$.

In summary, $U_d$(Dirac) is superior to $U_d$(WS) for the deuteron scattering from $^{58}Ni$ at 400 MeV at forward angles up to 15°, while the two type of the potential give almost the same quality of fit to the data on the proton scattering. This indicates that the deuteron scattering can be a good probe to remove the ambiguity of the proton optical potential and that the folding potential $U_d$(Dirac) is useful at the forward angles. The success of $U_d$(Dirac) stems from its real central part which has a wine-bottle shape and a weak attraction. At backward angles around 30°, $U_d$(Dirac) understimates the observed cross section by a factor of 3 as shown in Fig.1. It should be noted, however, that the absolute magnitude of the cross section there is down from that at, say, 5° by a factor of $10^6$. Thus, one expects minor corrections of that sort of order of magnitude can affect the calculated results. Among them is the correction due to the deuteron breakup effects. An actual calculation with the coupled-channels method[3] shows that the s-wave breakup process enhances the calculated cross section to half the observed one around 30°. In contrast, the effect is negligible compared to the main contribution of the folding model at angles up to 15°.

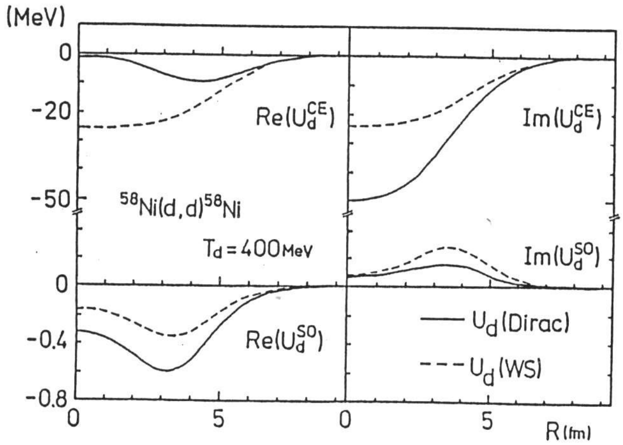


Figure 3.

Radial dependence of the folding potentials for $^{58}Ni(d,d)^{58}Ni$ at 400 MeV.
The solid line represents $U_d$(Dirac) and the dashed line $U_d$(WS).

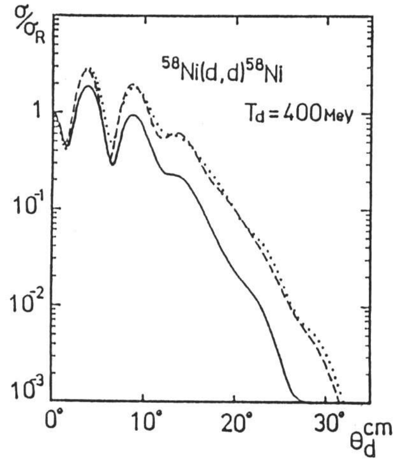


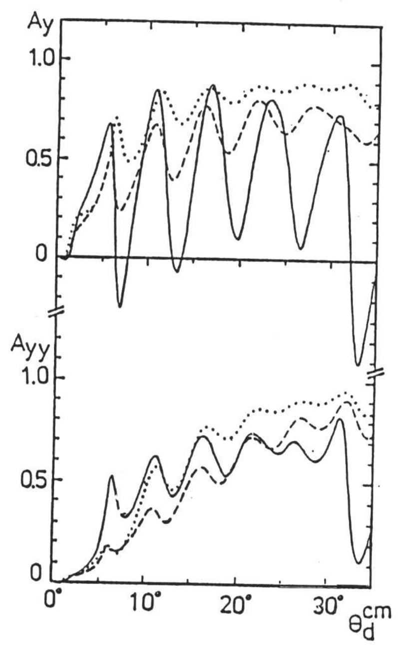


Figure 4.

Theoretical cross section and vector- and tensor-analyzing powers in $^{58}Ni(d,d)^{58}Ni$ at $T_d$=400 MeV. The role of the real central part of $U_d$(Dirac) is investigated. The solid line represents the result of $U_d$(WS) with its real central part replaced by that of $U_d$(Dirac). The dashed line represents the result of $U_d$(WS) but with the imaginary central part of $U_d$(Dirac) and the dotted line corresponds to $U_d$(WS) but with spin-orbit part of $U_d$(Dirac).

Acknowledgements
The authors wish to express their thanks to Dr. T. Hasegawa for his valuable discussions concerning the data of Ref.5. They also wish to thank Dr. Y. Sakuragi for useful discussions. The numerical calculations were done at the Computer Center of Kyushu University with the financial support from the Research Center for Nuclear Physics, Osaka University.

References

1) S.Watanabe: Nucl.Phys. 8 (1958) 484.
2) F.G.Perey and G.R.Satchler: Nucl.Phys. A97 (1967) 515.
3) M.Yahiro, M.Nakano, Y.Iseri and M.Kamimura: Prog.Theor.Phys. 67 (1982) 1467. and references therein.
4) N.van Sen et al.: Phys.Lett. 156B (1985) 185.
T.Hasegawa: private communications.
5) R.V.Reid: Ann. Phys. 50 (1968) 411.
6) G.S.Blanpied et al.: Phys.Rev. C18 (1978) 1436.
W.R.Coker, L.Ray and G.W.Hoffmann:Phys.Lett. 64B (1976) 403.
7) P.Schwandt et al.: Phys.Rev. C26 (1982) 55.
8) A.Ingemarsson et al.: Nucl.Phys. A365 (1981) 426.
9) L.G.Arnold et al.: Phys.Rev. C23 (1981) 1949.
10) B.C.Clark et al.: Phys.Rev. C31 (L985) 694; C31 (1985) 1975 (Erratum).

DISCUSSION

SANTOS: The use of a folding model for the deuteron presupposes that we can separate the center of mass motion from the relative motion. However we do not know how to make this separation in a fully relativistic way. Therefore the justification for using the (non-relativistic) folding of Dirac nucleon potentials over the deuteron wave function is not entirely clear.

MORAVCSIK: I am surprised that you find more difference between the two potentials at small angles, which correspond to large distances while the two potentials differ mainly at small distances.

YAHIRO: Two types of folding potentials are different from each other at distances smaller than 6 fm. The scattering around 15° does not corresponds to the potential at distances larger than 6 fm, since the transferred momentum of the scattering is about 2 $fm^{-1}$ which corresponds to a distance at $R \simeq 2\pi/2 \simeq 3$ fm.